Thin Solid Films 771 (2023) 139781

Contents lists available at ScienceDirect

Thin Solid Films

journal homepage: www.elsevier.com/locate/tsf

Controlling the optical properties of hafnium dioxide thin films deposited with electron cyclotron resonance ion beam deposition

Chalisa Gier [a], Marwa Ben Yaala [a,*], Callum Wiseman [a], Sean MacFoy [a], Martin Chicoine [c], François Schiettekatte [c], James Hough [b], Sheila Rowan [b], Iain Martin [b], Peter MacKay [d], Stuart Reid [a]

[a] SUPA, Department of Biomedical Engineering, University of Strathclyde, Glasgow G1 1QE, United Kingdom
[b] SUPA, Institute for Gravitational Research, University of Glasgow, Glasgow G12 8QQ, United Kingdom
[c] Département de Physique, Université de Montréal, Montréal, QC H3T 1J4, Canada
[d] GOOCH & HOUSEGO PLC, Dowlish Ford, Ilminster TA19 0PF, United Kingdom

ARTICLE INFO

Keywords:
Ion beam deposition
Electron cyclotron resonance
Hafnium oxide thin films
Refractive Index
Bandgap energy
Amorphous thin films

ABSTRACT

The effects of reactive and sputtering oxygen partial pressure on the structure, stoichiometry and optical properties of hafnium oxide (HfO_2) thin films have been systematically investigated. The electron cyclotron resonance ion beam deposition (ECR-IBD) technique was used to fabricate the films on to JGS-3 fused silica substrates. The amorphous structure of HfO_2 films were determined by X-ray Diffraction. Energy-dispersive X-ray Spectroscopy and Rutherford Backscattering Spectrometry were carried out for the composition and stoichiometry analysis, where this suggests the formation of over-stoichiometric films. The data suggests that the O:Hf ratio ranges from 2.4 – 4.45 to 1 for the ECR-IBD fabricated HfO_2 films in this study. The transmission and reflectance spectra of the HfO_2 films were measured over a wide range of wavelengths ($\lambda = 185 – 3000$ nm) by utilizing a spectrophotometer. The measured spectra were analyzed by an optical fitting software, which utilizes the model modified by O'Leary, Johnson and Lim, to extract the optical properties, refractive index (n) and the bandgap energy (E_0). By varying the reactive and sputtering oxygen partial pressure, the optical properties were found to be $n = 1.70 – 1.91$, and $E_0 = 5.6 – 6.0$ eV. This study provides a flexible method for tuning the optical properties of HfO_2 coatings by controlling the mixture of reactive and sputtering gas.

1. Introduction

Hafnium oxide, also known as Hafnia (HfO_2), is one of the most attractive high refractive index materials, high-k dielectric, with excellent thermal and chemical stability [1] that are widely used in optical coating applications. They are also commonly used in multilayer optical coatings as the high index material, alongside low index material like silica, where it can be utilized in interference filters, anti-reflective coatings, metal-oxide-semiconductor transistors, and cameras that can be utilized for space applications [2–4]. Other applications that HfO_2 films has been utilized aside for optical coatings are memory applications [1,5,6], ferroelectrics transistors which can be used for in-memory computing devices, as well as neuromorphic devices [7–9] and as HfO_2 based nanoagent in clinical trials for radiosensitized tumor therapy [10]. HfO_2 has optical transparency over a wide spectral range, from ultraviolet (UV) to mid-infrared (mid-IR) region, due to its wide bandgap of 5.3 – 5.7 eV [11,12], alongside high laser induced damage threshold (LIDT), allowing it to often be utilized as the coating for optics in high power laser systems. These HfO_2 coated optics are utilize in filters or mirrors for laser spectroscopy, laser diodes, and multilayer high reflection mirrors for Gravitational-wave interferometers, for example [13–15]. Although, from previous studies by many authors over the years, it shows that HfO_2 has its favorable and advantages characteristics for different applications, but the optical and structural properties of the thin films can vary depending on the deposition methods, as well as the deposition parameters [1,2]. This leads to common deposition techniques, including electron beam evaporation [11,16,17], dual ion beam sputtering [18,19], reactive low voltage ion plating, radio frequency (RF) magnetron sputtering [20], high pressure reactive sputtering [21], pulsed laser deposition [1], and ion beam deposition (IBD)

* Corresponding author.
E-mail address: marwa.ben-yaala@strath.ac.uk (M. Ben Yaala).

https://doi.org/10.1016/j.tsf.2023.139781
Received 13 July 2022; Received in revised form 23 February 2023; Accepted 27 February 2023
Available online 5 March 2023
0040-6090/© 2023 The Author(s). Published by Elsevier B.V. This is an open access article under the CC BY license (http://creativecommons.org/licenses/by/4.0/).

[22,23], yielding inconsistent optical, electronic and structural properties. These inconsistencies reported in literature includes differences in films' stoichiometry due to the deposition method, crystalline phases, polycrystallinity, amorphous nature, density, and defect states [1,24,25]. With these inconsistencies reported in film properties, it has previously been demonstrated that IBD is a technique that is capable of the fabrication of high quality thin films, with properties close to those of bulk materials. The high quality includes low scattering, high density, high refractive index, low absorption, good mechanical structural properties, and good environmental stability. The investigation of the purity, stoichiometric defects, and optical properties are of great significance for the preparation of high-quality coatings.

Reported here is a strategy for the optimization of HfO_2 film properties by controlling the oxygen to argon ratio during the IBD process. The films were produced by utilizing electron cyclotron resonance (ECR)-IBD, which is a process that has previously yielded the lowest IR absorption in amorphous silicon thin films [26], but otherwise underexplored for optical coating development. The stoichiometry and elemental analysis of the films discussed were carried out by Energy-dispersive X-ray Spectroscopy (EDS) along with Rutherford backscattering spectrometry (RBS). The structural properties of the films were determined by X-ray Diffraction (XRD), and the optical properties, such as refractive index (n) and bandgap energy (E_0), were obtained by fitting the transmittance and reflectance spectra by using a commercial optical fitting software application. The aim of this work is to report the correlation between the reactive oxygen partial pressure and HfO_2 films' optical and structural properties and film composition by utilizing the ECR-IBD technique.

2. Materials and method

2.1. Thin film fabrication

The HfO_2 coatings presented in this study were fabricated in a custom-built IBD system [26], utilizing three compact ECR ion sources (all ECR sources from *Polygon Physics, France*), as shown in Fig. 1. These ion sources generate highly confined (mm-scale) parallel beams extracted through a single aperture and extracted with 10 kV potential. The three ion beams are directed onto a HfO_2 target, which is situated in the middle of the chamber. During the deposition process, everything inside the system was kept constant (i.e. target-to-substrate position, target angle, etc.). The ion sources parameters are controlled via a LabVIEW software (Version 16.0, NI): gas flow through the ion sources, the individual microwave power for plasma generation, beam voltage, and focus voltage. The microwave power input is between 3 – 5 W, the focus voltage is between 3 – 6 kV and the beam voltage is kept constant at 10 kV for all sources. The chosen parameters are used to provide the highest extraction current, minimal beam divergence, highest ion energies and to provide the most stable beam for each deposition.

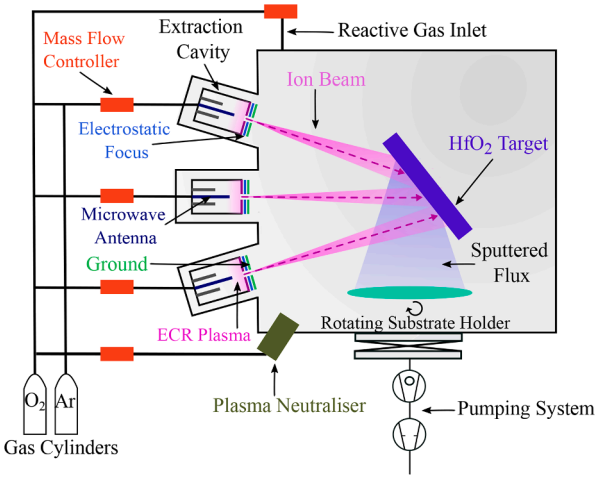

Fig. 1. Schematic diagram of the experimental setup for the HfO_2 study. The figure shows all the different components of the custom-built ECR-IBD system.

The substrates used in this study are JGS-3 fused silica circular discs, 20-mm in diameter and 1-mm thick (*Changchun Qianhao Photoelectric Co., Ltd, China*). For improved thickness uniformity of the coatings, four samples are placed on a rotating substrate holder, on a ferrofluidic drive, driven by a stepper motor at 0.6 rpm for each deposition. Due to the nature of the ECR sources and their low deposition rate (~0.01 Å/s), the deposition time for each run is 72 h, where the thickness varies between 140 – 270 nm, dependent on the coating configurations. The growth rate was measured *in situ* by utilizing a quartz microbalance, and the thickness of the coatings were later determined by fitting the transmittance and reflectance measurements using SCOUT (Version 4.93, WTheiss Hardware and Software).

A hafnium oxide target with 99.99% purity was used for this investigation. A neutralizer was added to the setup to mitigate instabilities associated with plasma charging build-up, in addition to electrical discharging/arcing due to the accumulation of charge on the non-conductive target surface.

For the deposition process, the base pressure of the chamber was lower than 3×10^{-4} Pa and the deposition were carried out at room temperature. The total pressure was fixed to 2.5×10^{-2} Pa during deposition. The gasses were introduced in the chamber following three configurations:

(i) Varying the reactive oxygen background partial pressure from 10% to 90% of the fixed total pressure value, where argon is introduced through the sources and neutralizer, where this will be referred to as '*X*% Reactive Oxygen'
(ii) Varying the sputtering oxygen partial pressure through 1 or 3 sources with no background gas, where this will be referred to as: '10% Sputtering Oxygen' when 1 source is utilizing oxygen while the remaining 2 sources and the neutralizer are utilizing argon; and '30% Sputtering Oxygen' when all 3 sources are utilizing oxygen and the neutralizer is utilizing argon. For this configuration, the argon from the neutralizer is taken into account for the overall gas percentages and fixed total pressure value
(iii) Using pure oxygen gas for the full process through the sources and the neutralizer, where this will be referred to as 'Pure Oxygen Process'

2.2. Optical characterization

For the optical characterization of the deposited films, Photon RT spectrophotometer (*EssentOptics Ltd., Belarus*) was used to obtain the transmittance (T) and reflectance (R) of the coatings at the wavelength range of 185 – 5000 nm. Once both spectra were obtained for each substrate, the data is imported to the optical fitting software SCOUT to analyze the spectra [26,27].

There are many different methods which can be used to model the optical properties of amorphous semiconductors, based on the density of states (DOS) function, where Tauc-Lorentz model [28] and O'Leary, Johnson, and Lim (OJL) model [29] are typically used. Within this study, the OJL model has been utilized within SCOUT.

OJL model is used to describe the interband transition in the amorphous semiconductors [30,31]. This model assumes the parabolic shape valance and conduction band of the DOS, with tail states exponentially decaying into the bandgap [29–31]. The said tail states are the results of the disorder present in amorphous semiconductor, where this is also known as the Urbach tail [32]. The parameters of OJL DOS model are:

$$E_{m,c} = E_c + \frac{1}{2}\gamma_c \tag{2.2.1}$$

$$E_{m,v} = E_v - \frac{1}{2}\gamma_v \tag{2.2.2}$$

Where E_c and E_v are the conduction and valence band energy, γ_c and γ_v is the damping constant of the conduction and valence bands, and m_c and m_v are the conduction and valence band mass. Eqs. (2.2.1) and 2.2.2 represents the mobility edges of the conduction and valence bands, respectively. As for the bandgap energy (E_0), this is denoted by:

$$E_c + \frac{1}{2}\gamma_c - \left[E_v - \frac{1}{2}\gamma_v\right] = E_0 \tag{2.2.3}$$

Where E_0 can be acquired via SCOUT. The other OJL interband transitions within SCOUT are as follows [30,31,33,34]:

- OJL mass: this acts as the scaling factor in determining the shape of the DOS
- OJL gamma valence: this is the band tail width, or Urbach tail
- OJL decay: this is the number which ensures the imaginary part decays to zero for high frequency

As for the refractive index (n), this is calculated by utilizing the Kramers-Kronig Relation (KKR) implemented in SCOUT. The KKR connects the real and imaginary parts of the susceptibilities, and can be used to calculate the real and imaginary parts of the dielectric function. By utilizing both the KKR and OJL model implemented in SCOUT and fitting of T and R spectra, this allows for the extraction of n, E_0, and thickness, among other optical constants not discussed in this study.

The following steps were taken within SCOUT to carry out the optical fittings: (1) Introduce the OJL model, initial values of the complex refractive index (based on literature) and film thickness. (2) Insert the T and R spectra. (3) Run the "automatic fit", where the downhill simplex method is applied to vary the fit parameters in order to minimize the deviation between the experimental and simulated values, until an optimal fit is obtained. (4) The E_0, n and thickness values can now be obtained [30,31].

2.3. Elemental and structural characterization

The compositional elemental analysis and mapping of the samples were measured by Hitachi S3700-N Scanning Electron Microscope (SEM), equipped with an EDS system at room temperature, operated at an accelerating voltage of 10 kV. Further confirmation of the elemental analysis were carried out by RBS measurements, which were carried out using a 2 MeV ^{4}He beam. The beam was incident at an angle of 7° from the surface of normal to minimize channeling effects, and the detector was placed at a scattering angle of 170° Atomic concentrations were determined by fitting the experimental spectra with the SIMNRA program [35]. The structure of the films was determined by utilizing XRD method using Bruker D8 Advance with a Cu Kα X-ray source at λ = 1.541 Å. The XRD scans are measured in the standard Bragg-Brentano geometry, measured between the angles of 2θ = 20 – 55°

3. Results

Fig. 2 shows the XRD pattern of pure HfO_2 films with varying oxygen content: (i) in the background with argon as the sputtering gas, (ii) through the ion sources (1 and 3 sources), where argon is still present in the process through the neutralizer, and (iii) pure oxygen process, where there is no argon inside the chamber. As can be seen from the XRD data, all HfO_2 films show a broad weak band, which indicates that all of the films in this study are amorphous. XRD data for a blank substrate is also included to show the peak centered at ~21° in all samples is from the substrate. The XRD data shows minimal difference between the blank substrate and coated substrates, which further demonstrates that the HfO_2 thin films in this experiment are amorphous. Also included in the figure is a sample annealed to 500 °C from the pure oxygen process,

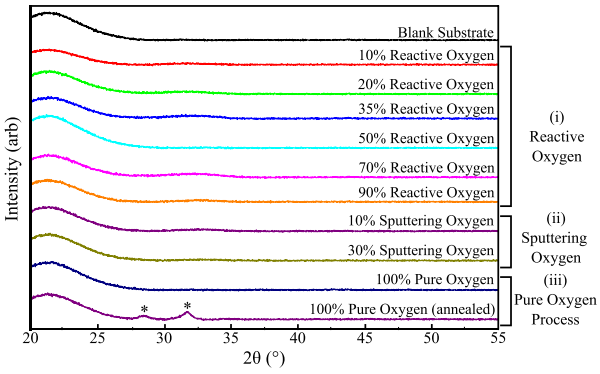

Fig. 2. XRD spectra of blank substrate and HfO_2 thin films deposited by ECR-IBD for the three different configurations of the introduction of oxygen in the system: (i) reactive gas, (ii) sputtering gas, and (iii) pure oxygen process with and without thermal annealing.

which shows the emergence of narrow peaks compared to the as-deposited films. These narrow peaks are an indicator to the increasing crystalline structure when the films are annealed, and are denoted by * in Fig. 2. This is further confirmation that the as-deposited samples investigated are in fact amorphous.

The atomic composition of the deposited hafnia films measured by EDS is shown in Fig. 3. The only elements detected by utilizing EDS in all coatings are O, Hf, and Ar. In Fig. 3a and b, the atomic percentage of oxygen and hafnium present in the films are provided. Fig. 3d shows the ratio between oxygen and hafnium present. By increasing the background oxygen partial pressure over 35%, an increase of the oxygen concentration in the films is observed. The highest value of oxygen concentration in the films was acquired by 30% sputtering oxygen, where the O:Hf ratio is 4.45:1 (*red circle*). Note that the composition for the pure oxygen process was not measured by EDS. From Fig. 3d, it can be seen that all coatings have an excess of oxygen, and are over-stoichiometric due to the measured O:Hf ratios being above 2:1, where the lowest is 2.4:1 at 20% background oxygen (*black square*). Fig. 3c shows the Ar atomic percentage measured by EDS. For all films within this study, the Ar concentration is lower than 2.5%. The decrease in Ar concentration is correlated with the oxygen increase, as shown in Fig. 3a. However, at 30% sputtering oxygen (*red circle*), there are no Ar incorporated within the films.

Due to the high O:Hf content shown in Fig. 3d, RBS measurements were also carried out to confirm the O:Hf content, and the stoichiometry of the films discussed within this paper. Fig. 4 shows the O:Hf content acquired by utilizing RBS method. As shown, the results are slightly different to that of EDS results (Fig. 3d). However, the RBS results are in agreement with EDS results, where the films discussed within this study are all over-oxygenated, and therefore, over-stoichiometric. As previously mentioned, for stoichiometric HfO_2 thin films, the O:Hf ratio must be 2:1, where in this case (based on RBS results, Fig. 4), the lowest O:Hf ratio in this study has the value of 2.65:1 at 10% background oxygen (*black square)*. Alongside, the highest O:Hf ratio in this study, based on RBS results, is 3.89:1 at pure oxygen process (*green triangle*).

The transmittance and reflectance measurements are shown in Fig. 5. The absorption peaks measured at 2700 nm (very predominant in the transmittance data) are the water absorption peaks, which are associated with the substrate material. As described in the materials and methods section, for varying oxygen content configuration (i) are shown as solid lines, where 10% and 90% reactive oxygen is shown in Fig. 5; configuration (ii) is shown as dashed lines; and configuration (iii) is shown as dotted lines. As shown in Fig. 5, the higher the oxygen content (for all three configurations), the transmittance also increases, and therefore, the reflectance decreases – where this can be seen most prominently in the range of 1500 – 3000 nm. In example, for configuration (i) 10% reactive oxygen (*red, solid line*) has a lower transmittance

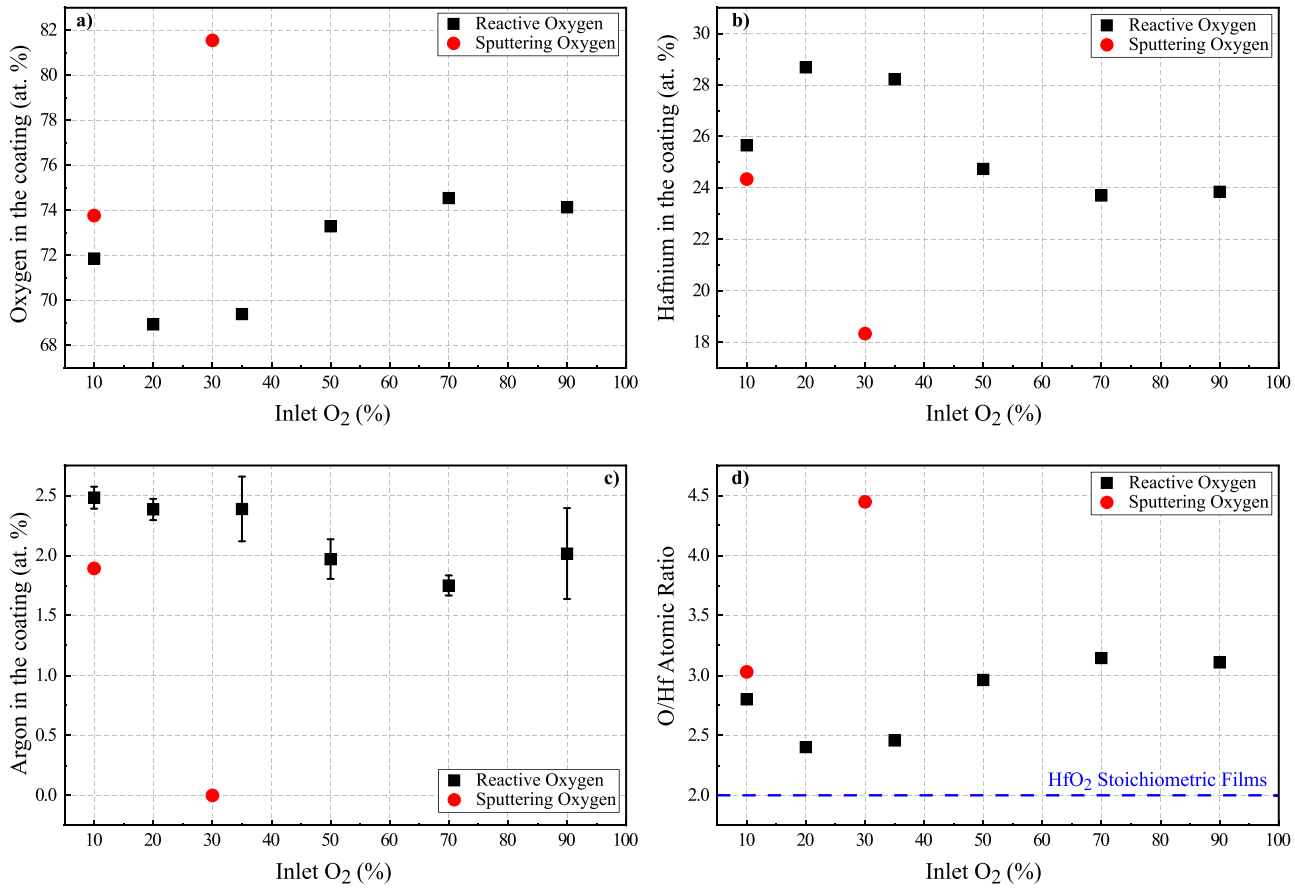

Fig. 3. EDS measurement of the atomic percentages of (a) oxygen, (b) hafnium, (c) argon in the coatings, and (d) atomic percentage ratio of oxygen over hafnium in the coatings.

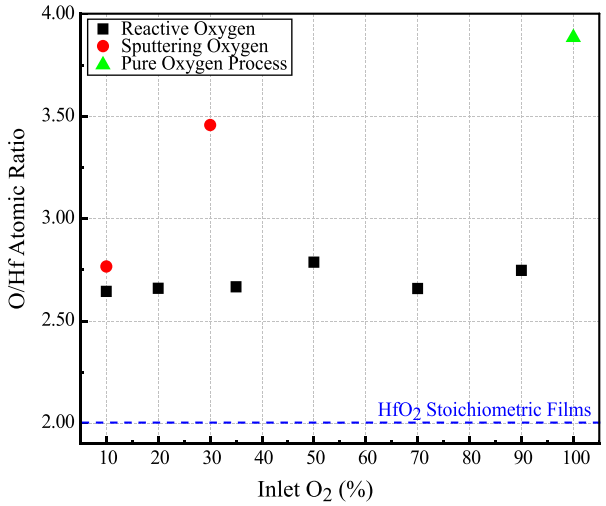

Fig. 4. Atomic percentage ratio of oxygen over hafnium in the coatings extracted by RBS measurements.

(and higher reflectance) than that of 90% reactive oxygen (*magenta, solid line*) in this wavelength range. This is also true for configuration (ii), where 10% sputtering oxygen (*blue, dashed line*) has a lower transmittance (and higher reflectance) than that of 30% sputtering oxygen (*green, dashed line*) within this wavelength range. Alongside, configuration (iii), where this is the pure oxygen process (*orange, dotted line*) has the highest transmittance, and lowest reflectance out of all three configurations.

It can also be observed that the transmittance data of samples shown exhibit interference effects. These interference fringes can be used as an indicator for the thickness of the films [31], where it can be observed that the films have different thickness due to the different configurations and oxygen percentages. As previously mentioned, all coatings have the same deposition time of 72 h, where the thicknesses varies between 140 – 270 nm, dependent on the coating configurations. From Fig. 5, the data shows that by varying the oxygen content, for all three configurations, this has an effect on the transmittance and reflectance data, along with other optical properties, which will be discussed further.

Fig. 6a shows the refractive index acquired from fitting via SCOUT for the wavelength range of 200–2500 nm, whereas Fig. 6b shows the refractive index extracted for a fixed wavelength of 1064 nm. This wavelength is chosen as Nd:YAG lasers operating at 1064 nm are widely used in many high power laser systems, including for military, medicine, and spectroscopy purposes. Fig. 6a shows that, as the oxygen concentration increases, the refractive index decreases for all three configurations (reactive oxygen, sputtering oxygen, and pure oxygen process), where the pure oxygen process possessing the lowest refractive index, and 10% reactive oxygen process possessing the highest refractive index. Fig. 6b also shows that at 10% reactive oxygen, the refractive index at 1064 nm is the highest ($n = 1.91$) and decreasing as the reactive oxygen percentage increases. The lowest refractive index at 1064 nm is for the pure oxygen process with the value of $n = 1.72$. The data shown in Fig. 6 are quoted from the average values from SCOUT fittings, where four coated substrates from each run are fitted five times each.

Fig. 7 shows the bandgap energy of HfO_2 films, extracted from the OJL gap energy model. For configuration (i) [*black square*], Fig. 7 shows that at 35% reactive oxygen partial pressure has the lowest bandgap energy of 5.6 eV, however, within the error range, from 10 – 50%

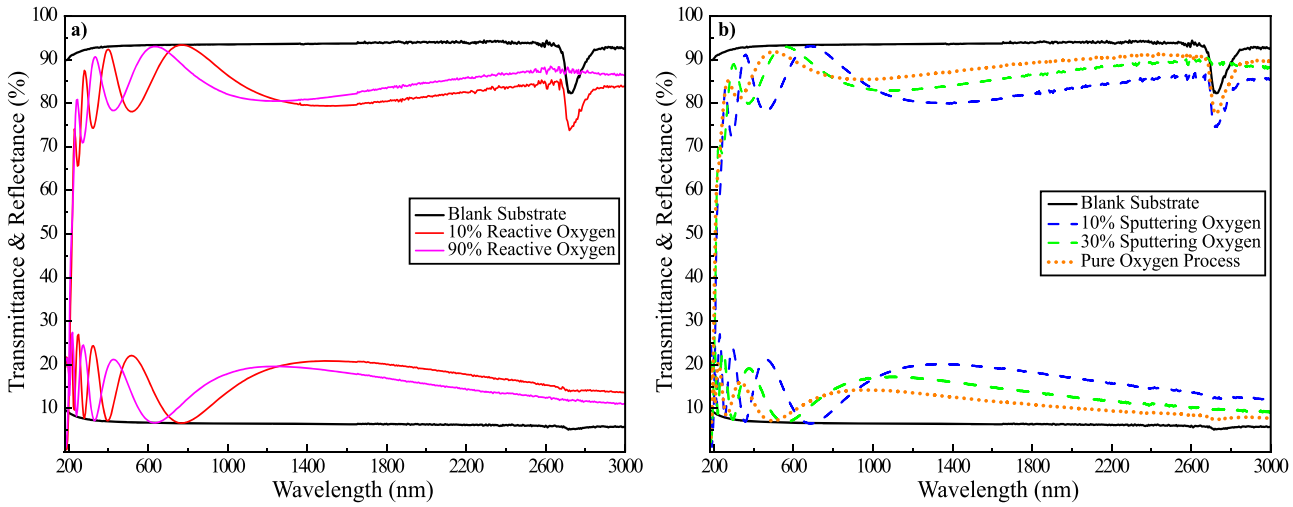

Fig. 5. Transmittance and reflectance data acquired from Photon RT spectrophotometer with wavelength range of λ = 185 – 3000 nm. Only a few selected samples used in this study are shown in the figure.

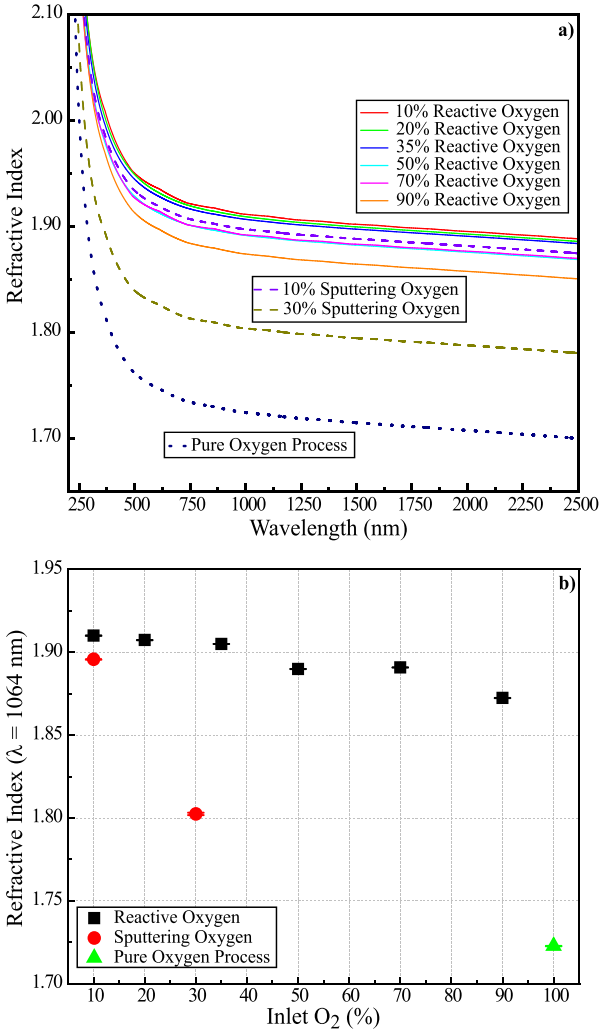

Fig. 6. Refractive index of the films acquired from SCOUT fittings: (a) dispersion of refractive index versus wavelength of HfO_2 films with different oxygen configurations, and (b) refractive index of each film at 1064 nm versus the oxygen percentage.

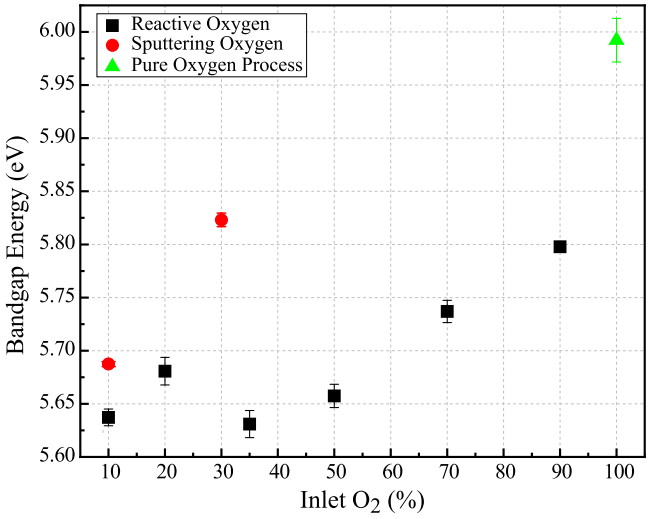

Fig. 7. OJL bandgap energy (E_0) versus oxygen percentage, where E_0 is acquired from the computed data from SCOUT.

reactive oxygen partial pressure, the bandgap energies are within the same values of 5.65 ± 0.05 eV. For configuration (ii) [*red circle*], the bandgap energy increases with the increasing percentage of oxygen used as sputtering gas, from 5.69 eV at 10% sputtering oxygen to 5.82 eV at 30% sputtering oxygen. As for configuration (iii) [*green triangle*], the pure oxygen process provides the highest bandgap energy at 6 eV. The overall trend that can be concluded from Fig. 7 is that as the oxygen concentration increases for each configuration, the bandgap energy also increases.

4. Discussion

The transmission spectra measured for all films presented in Fig. 5 show a high transmission from the UV to mid-IR (~300–3000 nm) which makes HfO_2 an interesting material for optical applications. At the wavelength of ~2700 nm, it can be seen that in the transmittance data, there are absorption peaks. This absorption is common in fused silica substrates, where this band corresponds to the OH absorption band (or "water band") [36]. It can also be seen that they are substrate-dependent, as not all of the transmittance data shown in Fig. 5 possess this absorption peak. As this absorption peak is only due to the

substrates, it is negligible when it comes to the discussion of the films optical constants in this study.

The XRD data in Fig. 2 shows that all coatings within this experiment exhibit a very broad wide band and minimal difference compared to blank substrates, which demonstrates that the HfO_2 films in this experiment are amorphous, similar to the amorphous glass substrate. The XRD data for annealed HfO_2 fabricated within the same pure oxygen process is shown to exhibit narrow peaks, where this shows that the film is becoming more crystalline in nature. This is in contrast to the broad peak of the films within this investigation, further verifying that the films are amorphous, even with the increase of oxygen content at room temperature.

The EDS compositional analysis presented in Fig. 3 shows that, within the measurement certainty of circa 0.1%, only Ar, O, and Hf species are observed. High purity films are expected from the ECR-IBD process, due to a highly confined, filament-free plasma generation in addition to the extraction of ions through a single aperture. The single aperture extraction allows high extraction potentials and eliminates the requirement for extraction grids that are a source of contamination in standard IBD processes. As shown in Fig. 3c, the films contain interstitial argon in the range 1.7 – 2.5%, which is typical in IBD processes, where inert gasses are used as the sputtering species, and trapped atoms can create "nanobubbles" [23]. However, the 30% sputtering oxygen process (configuration (ii), where argon is only utilized via the neutralizer) and pure oxygen process (configuration (iii), based on RBS results), does not have any Ar within the films, due to no use of argon during the deposition process. The amount of Ar that exists within the films in this study is slightly higher than the Ar solubility in solid materials (~1%) [23,37], however, this is still less than that of conventional RF-IBD systems (6 – 10%) [23]. This surplus of Ar quantity is associated with the implantation of the reflected neutral atoms with high kinetic energies, where the backscattered argon are incorporated into the coatings, along with the film-forming particles, as the angular distribution of each of these have some overlap as they leave the target surface [23,38,39]. These Ar atoms will accumulate to form bubbles within the HfO_2 matrix due to the inert nature of the gas. Whilst the fraction of argon in these samples are low, the quantity of implanted argon bubbles [23] decreases with increasing oxygen adsorption in the films. It is likely that the different oxygen regimes across the range of the samples reported in this paper play different roles in the deposition process and resultant thin film properties. The presence of nanobubbles, both due to the entrapment of Ar and O_2 molecules, may have an effect on the absorption of thin films, alongside the LIDT if used in laser systems, as the trapped nanobubbles can lead to optical breakdown due to laser exposure. Further investigation into the nanobubbles and the effect on absorption and LIDT results produced by films utilizing ECR-IBD will be of interest to study.

In addition, from both the EDS measurements and RBS measurements, the films presented in this paper are all over-stoichiometric in relation to the composition of the HfO_2 target (2:1 is the expected O:Hf ratio). Different mechanisms are thought to be the cause for the over-stoichiometry:

(I) Interstitial oxygen in the films, where the oxygen molecules are supplanted in the interstitial sites within the HfO_2 lattice, where the oxygen aggregates in the films [40];
(II) Higher coordination number compounds are bonded during the deposition due to the high energy process (e.g. HfO_x, where $x > 2$) [41].

Since Hf does not have a stable oxidation state to allow for bonding of three O atoms, the possibility of higher coordination compound like HfO_3 can be ruled out. In turn, this leads to the conclusion that the over-stoichiometry observed are due to the interstitial oxygen within the films.

The decreasing refractive index of the films at higher reactive oxygen partial pressure (Fig. 6), where the literature value reported is $n = 1.88$ at 1064 nm for HfO_2 thin films, and $n = 2.1$ (at 550 nm) for bulk HfO_2 [11,42–44] can be attributed to the interstitial oxygen that exists within the lattice. Alongside the decrease in refractive index observed due to interstitial oxygen, this also leads to the increasing bandgap behavior (Fig. 7), particularly increasing to greater than the reported bandgap values (5.3 – 5.7 eV) [11,12].

With the increase of oxygen content and O:Hf ratios, changes can be observed most prominently in the increased transmittance data (Fig. 5), especially in the mid-IR region of the samples deposited ($\lambda \approx 1300$ – 3000 nm). At 90% reactive oxygen (configuration (i)), where the O:Hf ratio is ~3:1, the transmittance has increased the most compared to other spectra in the same configuration (i), (Fig. 5a). At 30% sputtering oxygen (configuration (ii)), where the O:Hf ratio is ~4.45:1 (from EDS, and ~3.5:1 from RBS), provides an even higher transmittance than that of reactive oxygen configuration; and the pure oxygen process (configuration (iii)), where this has the highest transmittance out of all three configurations (Fig. 5b) with O:Hf ratio of ~4:1 (Fig. 4, *green triangle*).

Fig. 6 shows that as the oxygen content increases, for all configurations, the refractive index decreases. This reduction in refractive index related to the increase of reactive oxygen partial pressure in configuration (i) could also be associated to the reduced packing density, which also leads to the increase in the bandgap energy when comparing between the samples within the same configuration. As previously stated, in literature, the refractive index of HfO_2 thin films is $n = 1.88$ at 1064 nm for HfO_2 thin films, where the films were fabricated by electron beam evaporation [11,42]. For films in configuration (i), the overall refractive index at differing reactive oxygen percentages is higher than reported values, where this could be due to the higher overall packing density through the use of ECR-IBD when compared to films fabricated by other processes, such as electron beam evaporation or magnetron sputtering, when the films are still amorphous. Fig. 6 also shows that the refractive index is lower when utilizing oxygen as sputtering gas compared to argon, where this is most apparent in the pure oxygen process (configuration (iii)).

As for the optical bandgap energy, this is affected by many factors: defect density, purities, packing density, stoichiometry, etc. As previously stated, the bandgap energy of HfO_2 reported in the literature is 5.3 – 5.7 eV [11,12]. It can be seen that in this work, by increasing the oxygen content during the deposition, the bandgap energy can be manipulated to be higher than that of the reported values (Fig. 7). Other researchers [13] have reported the values of 5.59 – 5.68 eV with increasing reactive oxygen partial pressure, and another group [45] have reported the values of 5.58 – 5.83 eV, where in this work, the values are reported in the range of 5.6 – 5.8 eV by increasing the reactive oxygen partial pressure (configuration (i)). As for configuration (ii) and (iii), the bandgap energies are in the range of 5.69 – 6.0 eV. This shows that as the oxygen content increases, the bandgap energy increases, which is in agreement with other groups' findings [45]. In addition, there is also a slight blue-shift of the transmittance data (Fig. 5), at the UV range for the absorption edge, that can be seen with the increase of oxygen content. This absorption edge is associated with the bandgap energy, and the shift seen is known as Burstein-Moss shift, where this shift to lower wavelengths of the absorption edge is associated with the increase of bandgap energy.

As stated earlier, the decrease in refractive index and increase of bandgap energy as the oxygen content increases within this study can also be due to the decrease in the packing density of the films. Yoldas formula [45] can be utilized to calculate the packing density (p), where this is defined as:

$$p = \frac{n_p^2 - 1}{n_b^2 - 1} \tag{4.1}$$

Where n_p is the refractive index of the thin films at 600 nm, and n_b is the refractive index of bulk-HfO_2 in this case, where $n_b = 2.1$. By

utilizing this equation, it was found that the highest packing density within this study can be found for 10% reactive oxygen (configuration (i)) where $p = 0.81$, and the lowest packing density within this study is found when utilizing pure oxygen process (configuration (iii)) where $p = 0.6$. This is in agreement with the results extracted from SCOUT, where at highest packing density calculated (10% reactive oxygen, configuration (i)), the refractive index is highest (Fig. 6), with the lowest bandgap energy (Fig. 7). Alongside, at lowest packing density calculated in this study (pure oxygen process, configuration (iii)), the refractive index is lowest (Fig. 6), with the highest bandgap energy (Fig. 7).

The film growth rate for all films sputtered with argon is ~0.01 Å/s, which is around two orders of magnitude lower than that of conventional IBD. The slow deposition rate may be one of the reasons for the over-stoichiometry where the oxygen adatoms have a longer time for reacting and diffusing in the forming thin film. The high energy of the ECR process could also produce highly reactive oxygen that sputters the targets and are bonded to the hafnium atoms. The rate decreases further with the introduction of oxygen in the sources as sputtering gas (configuration (ii) and (iii)). This rate is directly related to the momentum transfer between the bombarding ions and the target atoms, which is directly correlated to the difference in atomic mass between the working gas and the target atoms. In particular, for Hf, the sputtering yield is ~3 times higher with Ar than with O_2 [46].

5. Conclusion

The effect of reactive oxygen partial pressure and sputtering oxygen through the ion sources plays an important role in the optical properties of HfO_2 thin films, fabricated by ECR-IBD technique. ECR gridless high-energy ion sources produced high-density pure hafnia films (with a lower backscattered Ar content at ~2.5% compared to the conventional IBD technique). The structural analysis carried out by XRD confirmed that all films within this study are amorphous. The compositional analysis demonstrated that the films in this study were all over-stoichiometric as the O:Hf ratio is higher than 2:1, even for reactive O_2 partial pressure as low as 10% from the total process pressure which was found to be 2.8:1. Further investigation into the over-stoichiometry were carried out by utilizing RBS, where the results are in agreement with EDS results, demonstrating over-stoichiometric films found in this study. By utilizing the OJL model implemented within SCOUT software, the refractive index were found to be in the range of $n = 1.70 – 1.91$, and the OJL bandgap energy were found to be in the range of $E_0 = 5.6 – 6.0$ eV for the different oxygen concentrations that were investigated. The results indicated that the refractive indices decreases with the increase of oxygen content within the chamber, whereas the bandgap energies increases. This shift of bandgap to higher energies can also be seen from the slight shift towards lower wavelengths (blue shift) in the transmittance measurement in the UV range as the oxygen content increases. From the optical characterizations, it was found that by controlling both the reactive and the sputtering oxygen concentration during deposition, the bandgap energy, and the refractive index, could be tuned to the desired value, depending on the application.

Future work will include chemical analysis to understand how the excess oxygen is incorporated in the films and how it affects the nature of the hafnia coatings deposited by the ECR-IBD method. Furthermore, as HfO_2 coatings are of interest for high-quality optical coatings for laser systems, LIDT studies will be carried out to compare the three different configurations discussed in this investigation. Along with this, the study of temperature treatment on these films will also be of interest to determine the optical, structural and the oxygen incorporation changes that may be observe, and in turn, the LIDT changes that may occur.

CRediT authorship contribution statement

Chalisa Gier: Conceptualization, Methodology, Software, Validation, Formal analysis, Investigation, Resources, Data curation, Writing – original draft, Writing – review & editing, Visualization. **Marwa Ben Yaala:** Conceptualization, Methodology, Validation, Investigation, Resources, Visualization, Writing – review & editing. **Callum Wiseman:** Validation, Formal analysis, Resources. **Sean MacFoy:** Software. **Martin Chicoine:** Validation, Formal analysis, Resources. **François Schiettekatte:** Validation, Formal analysis, Resources. **James Hough:** Funding acquisition. **Sheila Rowan:** Funding acquisition. **Iain Martin:** Funding acquisition. **Peter MacKay:** Funding acquisition. **Stuart Reid:** Supervision, Writing – review & editing.

Declaration of Competing Interest

The authors declare that they have no known competing financial interests or personal relationships that could have appeared to influence the work reported in this paper.

Data availability

Data will be made available on request.

Acknowledgments

The authors would like to acknowledge that the EDS and XRD work were carried out at the Advanced Materials Research Laboratory (AMRL), at the University of Strathclyde. This work was supported by the Science and Technology Facilities Council [grant numbers ST/S001832/1, ST/T003367/1], the University of Strathclyde, the University of Glasgow, and Gooch and House Ltd.

References

[1] L. Sun, J.G. Jones, J.T. Grant, N.R. Murphy, C.V. R.amana, K.G. Eyink, J.P. Vernon, P.R. Stevenson, Nanoscale-thick thin films of high-density HfO2 for bulk-like optical responses, ACS Appl. Nano Mater 4 (2021) 10836–10844, https://doi.org/10.1021/acsanm.1c02267.

[2] S. Fang, C. Ma, W. Liu, J. He, C. Wang, G. Chen, D. Liu, R. Zhang, Effect of oxygen flow on the optical properties of hafnium oxide thin films by dual-ion beam sputtering deposition, Appl. Phys. A Mater. Sci. Process. 128 (2022), https://doi.org/10.1007/s00339-022-06224-2.

[3] D. Wernham, A. Piegari, Optical Coatings in the Space Environment, Elsevier LTD., 2018, https://doi.org/10.1016/B978-0-08-102073-9.00022-9.

[4] A. Wiatrowski, A. Obstarczyk, M. Mazur, D. Kaczmarek, D. Wojcieszak, Characterization of HfO2 optical coatings deposited by MF magnetron sputtering, Coatings 9 (2019) 1–20, https://doi.org/10.3390/COATINGS9020106.

[5] C. Künneth, R. Materlik, M. Falkowski, A. Kersch, Impact of four-valent doping on the crystallographic phase formation for ferroelectric HfO2 from first-principles: implications for ferroelectric memory and energy-related applications, ACS Appl. Nano Mater. 1 (2018) 254–264, https://doi.org/10.1021/acsanm.7b00124.

[6] M.H. Park, Y.H. Lee, T. Mikolajick, U. Schroeder, C.S. Hwang, Review and perspective on ferroelectric HfO2-based thin films for memory applications, MRS Commun. 8 (2018) 795–808, https://doi.org/10.1557/mrc.2018.175.

[7] H. Joh, M. Jung, J. Hwang, Y. Goh, T. Jung, S. Jeon, Flexible ferroelectric hafnia-based synaptic transistor by focused-microwave annealing, Cite This ACS Appl. Mater. Interfaces. 14 (2022) 1326–1333, https://doi.org/10.1021/acsami.1c16873.

[8] I.-.J. Kim, J.-.S. Lee, Ferroelectric transistors for memory and neuromorphic device applications, Supariyanto Dan Rosad 5 (2020) (2015) 248–253, https://doi.org/10.1002/adma.202206864.

[9] Z. Li, T. Wang, Y. Liu, J. Yu, J. Meng, P. Liu, K. Xu, H. Zhu, Q. Sun, D.W. Zhang, L. Chen, Understanding the effect of oxygen content on ferroelectric properties of Al-doped HfO 2 thin films, (2022) 9–12. 10.1109/LED.2022.3226195.

[10] Y. Li, Y. Qi, H. Zhang, Z. Xia, T. Xie, W. Li, D. Zhong, H. Zhu, M. Zhou, Gram-scale synthesis of highly biocompatible and intravenous injectable hafnium oxide nanocrystal with enhanced radiotherapy efficacy for cancer theranostic, Biomaterials 226 (2020), 119538, https://doi.org/10.1016/J.BIOMATERIALS.2019.119538.

[11] M.F. Al-Kuhaili, S.M.A. Durrani, E.E. Khawaja, Characterization of hafnium oxide thin films prepared by electron beam evaporation, J. Phys. D. Appl. Phys. 37 (2004) 1254–1261, https://doi.org/10.1088/0022-3727/37/8/015.

[12] E. Bersch, S. Rangan, R.A. Bartynski, E. Garfunkel, E. Vescovo, Band offsets of ultrathin high-κ oxide films with Si, Phys. Rev. B. 78 (2008), 085114, https://doi.org/10.1103/PhysRevB.78.085114.

[13] S. Jena, R.B. Tokas, S. Tripathi, K.D. Rao, D.V. U.dupa, S. Thakur, N.K. Sahoo, Influence of oxygen partial pressure on microstructure, optical properties, residual

stress and laser induced damage threshold of amorphous HfO2 thin films, J. Alloy. Compd. 771 (2019) 373–381, https://doi.org/10.1016/j.jallcom.2018.08.327.
[14] D. Schiltz, D. Patel, C. Baumgarten, B.A. Reagan, J.J. Rocca, C.S. Menoni, Strategies to increase laser damage performance of Ta_2O_5/SiO_2 mirrors by modifications of the top layer design, Appl. Opt. 56 (2017) C136, https://doi.org/10.1364/ao.56.00c136.
[15] Z. Balogh-Michels, I. Stevanovic, A. Borzi, A. Bächli, D. Schachtler, T. Gischkat, A. Neels, A. Stuck, R. Botha, Crystallization behavior of ion beam sputtered HfO2 thin films and its effect on the laser-induced damage threshold, J. Eur. Opt. Soc. Publ. 17 (2021), https://doi.org/10.1186/s41476-021-00147-w.
[16] L. Gallais, M. Commandré, Laser-induced damage thresholds of bulk and coating optical materials at 1030nm, 500 fs, Appl. Opt. 53 (2014) A186, https://doi.org/10.1364/ao.53.00a186.
[17] A. Hervy, L. Gallais, D. Mouricaud, G. Chériaux, Electron-beam deposited materials for high-reflective coatings: femtosecond LIDT, Opt. InfoBase Conf. Pap. (2013) 4–6, https://doi.org/10.1364/oic.2013.fa.4.
[18] L. Gallais, B. Mangote, M. Zerrad, M. Commandré, A. Melninkaitis, J. Mirauskas, M. Jeskevic, V. Sirutkaitis, Laser induced damage of hafnia coatings as a function of pulse duration in the femto to picosecond regime, Opt. InfoBase Conf. Pap. (2010), https://doi.org/10.1364/oic.2010.fa7.
[19] A. Ciapponi, F.R. Wagner, S. Palmier, J.Y. Natoli, L. Gallais, Study of luminescent defects in hafnia thin films made with different deposition techniques, J. Lumin. 129 (2009) 1786–1789, https://doi.org/10.1016/j.jlumin.2009.02.026.
[20] L. Pereira, P. Barquinha, E. Fortunato, R. Martins, Influence of the oxygen/argon ratio on the properties of sputtered hafnium oxide, Mater. Sci. Eng. B Solid-State Mater. Adv. Technol. 118 (2005) 210–213, https://doi.org/10.1016/j.mseb.2004.12.030.
[21] F.L. Martínez, M. Toledano-Luque, J.J. Gandía, J. Cárabe, W. Bohne, J. Röhrich, E. Strub, I. Mártil, Optical properties and structure of HfO2 thin films grown by high pressure reactive sputtering, J. Phys. D. Appl. Phys. 40 (2007) 5256–5265, https://doi.org/10.1088/0022-3727/40/17/037.
[22] G. Abromavičius, S. Kičas, R. Buzelis, High temperature annealing effects on spectral, microstructural and laser damage resistance properties of sputtered HfO2 and HfO2-SiO2 mixture-based UV mirrors, Opt. Mater. 95 (2019), https://doi.org/10.1016/j.optmat.2019.109245 (Amst).
[23] C. Harthcock, S.R. Qiu, R.A. Negres, J.A. Hammons, T. Voisin, G. Guss, A. A. Martin, C.J. Stolz, M.G. Menor, G. Bhowmik, M. Huang, The impact of nano-bubbles on the laser performance of hafnia films deposited by oxygen assisted ion beam sputtering method, Appl. Phys. Lett. 115 (2019), https://doi.org/10.1063/1.5129454.
[24] T.J. Bright, J.I. Watjen, Z.M. Zhang, C. Muratore, A.A. Voevodin, Optical properties of HfO2 thin films deposited by magnetron sputtering: from the visible to the far-infrared, Thin Solid Films 520 (2012) 6793–6802, https://doi.org/10.1016/j.tsf.2012.07.037.
[25] J. Aarik, H. Mändar, M. Kirm, L. Pung, Optical characterization of HfO2 thin films grown by atomic layer deposition, Thin Solid Films 466 (2004) 41–47, https://doi.org/10.1016/j.tsf.2004.01.110.
[26] R. Birney, J. Steinlechner, Z. Tornasi, S. Macfoy, D. Vine, A.S. Bell, D. Gibson, J. Hough, S. Rowan, P. Sortais, S. Sproules, S. Tait, I.W. Martin, S. Reid, Amorphous silicon with extremely low absorption: beating thermal noise in gravitational astronomy, Phys. Rev. Lett. 121 (2018), 191101, https://doi.org/10.1103/PhysRevLett.121.191101.
[27] W. Theiss, (2022) SCOUT software. http://www.wtheiss.com/.
[28] G.E.U. Jellison, Spectroscopic ellipsometry data analysis: measured versus calculated quantities, Thin Solid Films 313314 (1998) 3339.
[29] S.K. O'Leary, S.R. Johnson, P.K. Lim, On the relationship between the distribution of electronic states and the optical absorption spectrum in amorphous semiconductors, Solid State Commun. 109 (1999) 589–594, https://doi.org/10.1016/S0038-1098(98)00605-X.
[30] A. Solieman, A.A. Abu-Sehly, Modelling of optical properties of amorphous selenium thin films, Phys. B Condens. Matter. 405 (2010) 1101–1107, https://doi.org/10.1016/j.physb.2009.11.014.
[31] A. Solieman, Extracting the optical parameters of thermally evaporated Se film by modelling of transmittance spectra: effect of heat treatment, J. Taibah Univ. Sci. 14 (2020) 470–478, https://doi.org/10.1080/16583655.2020.1746600.
[32] F. Urbach, The long-wavelength edge of photographic sensitivity and of the electronic absorption of solids [8], Phys. Rev. 92 (1953) 1324, https://doi.org/10.1103/PhysRev.92.1324.
[33] N. Musila, M. Munji, J. Simiyu, E. Masika, R. Nyenge, Optical properties and analysis of OJL model's electronic inter-band transition parameters of TiO2 films, Path Sci. 4 (2018) 3001–3012, https://doi.org/10.22178/pos.36-5.
[34] A. Solieman, A.A. Abu-Sehly, Determination of the optical constants of amorphous AsxS 100-x films using effective-medium approximation and OJL model, Mater. Chem. Phys. 129 (2011) 1000–1005, https://doi.org/10.1016/j.matchemphys.2011.05.047.
[35] M. Mayer, SIMNRA user's guide, Report IPP 9/113, Max-Planck-Institut für Plasmaphysik, Garching, Germany, (1997). http://home.mpcdf.mpg.de/~mam/Report-IPP-9-113.pdf.
[36] A.M. Efimov, V.G. Pogareva, A.V. S.hashkin, Water-related bands in the IR absorption spectra of silicate glasses, J. Non. Cryst. Solids 332 (2003) 93–114, https://doi.org/10.1016/j.jnoncrysol.2003.09.020.
[37] M.R. Carroll, E.M. Stolper, Argon solubility and diffusion in silica glass: implications for the solution behavior of molecular gases, Geochim. Cosmochim. Acta 55 (1991) 211–225, https://doi.org/10.1016/0016-7037(91)90412-X.
[38] R. Feder, C. Bundesmann, H. Neumann, B. Rauschenbach, Ion beam sputtering of Ag - Angular and energetic distributions of sputtered and scattered particles, Nucl. Instrum. Methods Phys. Res. Sect. B Beam Interact. with Mater. Atoms. 316 (2013) 198–204, https://doi.org/10.1016/j.nimb.2013.09.007.
[39] C. Bundesmann, H. Neumann, Tutorial: the systematics of ion beam sputtering for deposition of thin films with tailored properties, J. Appl. Phys. 124 (2018), https://doi.org/10.1063/1.5054046.
[40] A.S. Foster, F. Lopez Gejo, A.L. Shluger, R.M. Nieminen, Vacancy and interstitial defects in hafnia, Phys. Rev. B - Condens. Matter Mater. Phys. 65 (2002) 1741171–17411713, https://doi.org/10.1103/PhysRevB.65.174117.
[41] J. Zhang, A.R. Oganov, X. Li, K.H. Xue, Z. Wang, H. Dong, Pressure-induced novel compounds in the Hf-O system from first-principles calculations, Phys. Rev. B - Condens. Matter Mater. Phys. 92 (2015) 1–10, https://doi.org/10.1103/PhysRevB.92.184104.
[42] M.F. Al-Kuhaili, Optical properties of hafnium oxide thin films and their application in energy-efficient windows, Opt. Mater. 27 (2004) 383–387, https://doi.org/10.1016/j.optmat.2004.04.014 (Amst).
[43] M. Jerman, Z. Qiao, D. Mergel, HfO2 as a function of the films ' mass density, Appl. Opy. 44 (2005) 3006–3012.
[44] D.L. Wood, K. Nassau, T.Y. Kometani, D.L. Nash, Optical properties of cubic hafnia stabilized with yttria, Appl. Opt. 29 (1990) 604, https://doi.org/10.1364/ao.29.000604.
[45] J. Gao, G. He, B. Deng, D.Q. Xiao, M. Liu, P. Jin, C.Y. Zheng, Z.Q. Sun, Microstructure, wettability, optical and electrical properties of HfO2 thin films: effect of oxygen partial pressure, J. Alloy. Compd. 662 (2016) 339–347, https://doi.org/10.1016/j.jallcom.2015.12.080.
[46] N. Matsunami, Y. Yamamura, Y. Itikawa, N. Itoh, Y. Kazumata, S. Miyagawa, K. Morita, R. Shimizu, H. Tawara, Energy dependence of the ion-induced sputtering yields of monatomic solids, At. Data Nucl, Data Tables 31 (1984) 1–80, https://doi.org/10.1016/0092-640X(84)90016-0.